

Adiabatic quantum computation with flux qubits, first experimental results.

S.H.W. van der Ploeg, A. Izmalkov, M. Grajcar, U. Hübner, S. Linzen, S. Uchaikin, Th. Wagner, A. Yu. Smirnov, A. Maassen van den Brink, M.H.S. Amin, A.M. Zagoskin, E. Il'ichev and H.-G. Meyer

(Invited Paper)

Abstract—Controllable adiabatic evolution of a multi-qubit system can be used for adiabatic quantum computation (AQC). This evolution ends at a configuration where the Hamiltonian of the system encodes the solution of the problem to be solved. As a first steps towards realization of AQC we have investigated two, three and four flux qubit systems. These systems were characterized by making use of a radio-frequency method. We designed two-qubit systems with coupling energies up to several kelvins. For the three-flux-qubit systems we determined the complete ground-state flux diagram in the three dimensional flux space around the qubits common degeneracy point. We show that the system's Hamiltonian can be completely reconstructed from our measurements. Our concept for the implementation of AQC, by making use of flux qubits, is discussed.

I. INTRODUCTION

THE concept of quantum computation by adiabatic evolution, i.e. Adiabatic Quantum Computation (AQC), was introduced by Farhi and coauthors [1]. It is an alternative to the “standard” concept of quantum computation where one has to construct a universal set of gates with long coherence times. As the latter requirement is not easy to achieve in superconducting quantum bits (qubits), presently the longest times achieved are of the order of several μs and only achieved at an optimal point [2], [3], AQC seems to be better as the system is only required to stay in the ground state. This led Kaminsky and co-authors to propose a scalable superconducting architecture for adiabatic quantum computation [4], where they make use of 3 Josephson Junction persistent current qubits [5].

In the AQC concept the solution of some non-polynomially (NP) hard problem is encoded into the ground state of a complex multi-qubit Hamiltonian H_P . The parameters of such a Hamiltonian can be controlled continuously so in this sense this method is similar to *analog* computation. The computation itself contains three majors steps: (A) preparation of the system

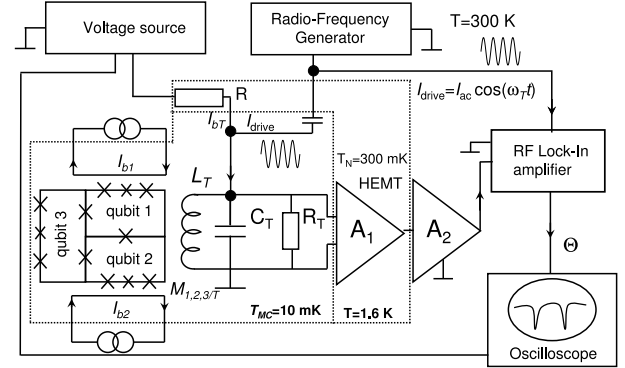


Fig. 1. Experimental setup for the demonstration of adiabatic quantum computation in a three-qubit-system, see section V. The qubits are coupled to a resonant tank circuit for the readout. The flux bias to the qubits is provided by a dc current I_{bT} applied to the coil L_T and bias currents $I_{b1,2}$ applied to additional bias wires, allowing full control over the individual qubits fluxes f_i . In the case of more qubits, more current sources would be used.

in a well-known state with Hamiltonian $H(t=0) = H_I$ at time $t=0$, (B) adiabatic evolution during the time interval t_{calc} towards the problem Hamiltonian H_P and (C) readout of the ground state of the problem Hamiltonian, which gives the answer. Therefore, in order to build a quantum computer based on AQC one has to be able to construct a qubit system with a controllable Hamiltonian and one has to be able to read out this system once the problem Hamiltonian H_P is encoded into it.

There has been an experimental implementation of an AQC algorithm in an NMR three-qubit quantum computer by Steffen *et al.* [6]. By using their computer they solve the so-called MAXCUT problem. This problem is one of the Non-Polynomially hard problems of Graph theory where the object of the problem is to find the maximal “cut” of a graph [7] and is mathematically equivalent to finding the ground state of some Ising-type Hamiltonian. Some of the authors have proposed how to implement and readout such an algorithm making use of flux qubits in a setup like the one shown in Fig.1 [8].

In this paper we review our recently obtained results from coupled flux qubits using our and implemented method for their characterization. Also we will show some of our results on multi qubit systems.

II. COUPLING OF QUBITS

In order to implement any protocol for quantum information processing, qubits should be coupled. Three Josephson

SvdP, AI and EI were supported by the RSFQubit and EuroSQIP projects, MG by Grants VEGA 1/2011/05 and APVT-51-016604.

S.H.W. van der Ploeg, A. Izmalkov, U. Hübner, S. Linzen, Th. Wagner, E. Il'ichev and H.-G. Meyer are at the Institute for Physical High Technology, P.O. Box 100239, D-07702 Jena, Germany

M. Grajcar is at the Department of Solid State Physics, Comenius University, SK-84248 Bratislava, Slovakia

S. Uchaikin, A. Yu. Smirnov, A. Maassen van den Brink and M.H.S. Amin are at D-Wave Systems Inc., 100-4401 Still Creek Drive, Burnaby, B.C., V5C 6G9 Canada

M.H.S. Amin and A.M. Zagoskin are at the Physics and Astronomy Dept., The University of British Columbia, 6224 Agricultural Rd., Vancouver, B.C., V6T 1Z1 Canada

A. Maassen van den Brink and A.M. Zagoskin are presently also at: Frontier Research System, RIKEN, Wako-shi, Saitama, 351-0198, Japan

junction persistent current flux qubits [5] can be coupled inductively just by placing them next to each other, however the achievable coupling strength is rather weak [9]. A larger coupling strength can be achieved by making use of the kinetic inductance of a common leg between them [10]. Even stronger coupling can be achieved by inserting a Josephson junction in this common leg [11]. The latter also provides the possibility of ferromagnetic coupling, whereas the other methods only provide anti-ferromagnetic coupling [12]. By insertion of an additional coupler loop between the qubits, one could realize controllable/switchable coupling between them [13]. This is particularly important for the realization of scalable superconducting architecture for AQC. Controllable coupling enables one to construct a Hamiltonian where both the energy bias ϵ_i and the coupling terms J_{ij} can be set *in-situ*.

A coupled N -flux-qubit system can be described by the Hamiltonian:

$$H_q = - \sum_i^N [\epsilon_i \sigma_z^{(i)} + \Delta_i \sigma_x^{(i)}] + \sum_{i < j} J_{ij} \sigma_z^{(i)} \sigma_z^{(j)}. \quad (1)$$

Here Δ_i is the tunneling amplitude, or half energy splitting, of qubit i at $f_i = 0$ and $\epsilon_i = \Phi_0 I_{p,i} f_i$ gives the energy bias applied to qubit i in terms of its persistent current $I_{p,i}$ and the normalized flux bias $f_i = \Phi_{x,i}/\Phi_0 - 1/2$ (Φ_0 is the flux quantum). The symbols $\sigma_x^{(i)}, \sigma_y^{(i)}, \sigma_z^{(i)}$ denote the Pauli matrices of the i -th qubit. The coupling energy is given by:

$$J_{ij} = \left(M_{ij} \pm \frac{\Phi_0}{2\pi I_{c,ij}} \right) I_{p,i} I_{p,j}, \quad (2)$$

where M_{ij} represents both the magnetic inductance between qubits i and j , as well as the kinetic inductance of a common leg. The second term describes the coupling due to an additional junction with critical current $I_{c,ij}$ inserted in the common leg between both qubits. The many-qubit system described by Eq. 1 can be characterized by the set of eigenstates $|\mu\rangle$ and eigenenergies $E_\mu, \mu = 1, \dots, 2^N$, which can be obtained from the solution of the equation: $H_q |\mu\rangle = E_\mu |\mu\rangle$. As an example the first two levels E_0 and E_1 are shown in Fig. 2 for a two qubit system with anti-ferromagnetic coupling ($J_{12} > 0$).

III. QUBIT READOUT USING A LOW-FREQUENCY RESONATOR

For the readout of the qubit system we use a high-quality LC resonator (tank-circuit) consisting of a superconducting coil with inductance L_T in parallel with a capacitance C_T [14]. In order to analyze the response of such a tank to the qubits we have to consider the complete Hamiltonian of the qubits system and readout resonator: $H = H_q + H_T + H_{\text{int}}$, where H_T is the Hamiltonian of the driven tank circuit and H_{int} the interaction term between tank and qubits. In principle, one should also add a term containing the dissipative interaction with the environment, which would result in line broadening, $\Gamma_{\mu\nu}$, of the many-qubit spectrum. However, the measurements are performed at a resonator frequency ω_T which is much less than the energy spacings, $\omega_{\mu\nu} = E_{\mu\nu} : \omega_T \ll |\omega_{\mu\nu}|$, of the coupled qubits. Under such non-resonant conditions the

effects of dissipation on the measurements are proportional to the small ratio $\Gamma_{\mu\nu}/|\omega_{\mu\nu}|$, and can be neglected.

The driven tank-circuit Hamiltonian can be written in terms of the non-commuting current, I_T and voltage, V_T operators. (here $[V_T, I_T]_- = -i\hbar\omega_T^2$, with $\omega_T = 1/\sqrt{L_T C_T}$ the resonance frequency) as:

$$H_T = \frac{C_T V_T^2}{2} + \frac{L_T I_T^2}{2} - L_T I_T I_{\text{drive}}, \quad (3)$$

where $I_{\text{drive}}(t) = I_{ac} \cos(\omega t)$ is the driving current of the tank. The interaction term is given by $H_{\text{int}} = -I_T \Phi$ with Φ the magnetic flux through the tank loop created by all qubits, $\Phi = \sum_i \lambda_i \sigma_z^{(i)}$. $\lambda_i = M_{iT} I_{p,i}$ is the coupling parameter between the i -th qubit and the tank, which is proportional to the mutual inductance between qubit and the coil of the tank-circuit M_{iT} and to the magnitude of the persistent current of the qubit. By using the Heisenberg equations $i\hbar \dot{V}_T = [V_T, H]_-$ and $i\hbar \dot{I}_T = [I_T, H]_-$ we obtain the following equation for the averaged current and voltage in the LC-circuit: $\langle \dot{I}_T \rangle = \langle V_T \rangle / L_T$,

$$\left(\frac{d^2}{dt^2} + \gamma_T \frac{d}{dt} + \omega_T^2 \right) \langle V_T \rangle = \frac{1}{C_T} \dot{I}_{\text{drive}} + \omega_T^2 \frac{d}{dt} \langle \Phi_{\text{tot}}(t) \rangle, \quad (4)$$

where the damping of the tank $\gamma_T = \omega_T / Q_T^0$ was added on an *ad-hoc* basis. The flux Φ_{tot} incorporates not only the flux Φ which the qubits would apply without their interaction with the tank, but also includes the response due to the tank according to:

$$\Phi_{\text{tot}} = \Phi(t) + (i/\hbar) \int_{-\infty}^t dt_1 [\Phi(t), \Phi(t_1)]_- I_T(t_1). \quad (5)$$

Here we have used the following notations for the (anti)commutator of two operators A and B: $[A, B]_{\pm} = AB \pm BA$, and the interaction picture.

Eq. 4 has the solution $\langle V_T(t) \rangle = V_T \cos(\omega t + \Theta)$ with Θ the phase shift of the voltage relative to the driving current. For the case of resonant driving, $\omega = \omega_T$, the voltage-current phase shift is determined by the sum, over all qubit combinations, of the real part of the qubit susceptibility χ'_{ij} :

$$\tan \Theta = -\frac{Q_T}{L_T} \sum_{ij} \lambda_i \lambda_j \chi'_{ij}(\omega_T). \quad (6)$$

The many-qubit susceptibility at the frequency of the tank $\omega_T, \omega_T \ll (E_\mu - E_\nu)/\hbar$ is calculated in the appendix and results in:

$$\chi'_{ij} = \sum_{\mu \neq \nu} \frac{\rho_\mu - \rho_\nu}{E_\mu - E_\nu} \langle \mu | \sigma_z^{(i)} | \nu \rangle \langle \nu | \sigma_z^{(j)} | \mu \rangle. \quad (7)$$

Here ρ_μ, ρ_ν denote the equilibrium occupation of the qubit energy eigenstates: $\rho_\mu = e^{-E_\mu/k_B T} / (\sum_\alpha e^{-E_\alpha/k_B T})$. A numerical calculation of the predicted response for a 2 qubit system is shown in Fig. 3. By comparing this with the energy diagram in Fig. 2 it is seen that the predicted signal is largest close to the anticrossings where the ground state E_0 has the largest curvature due to the superposition of flux states.

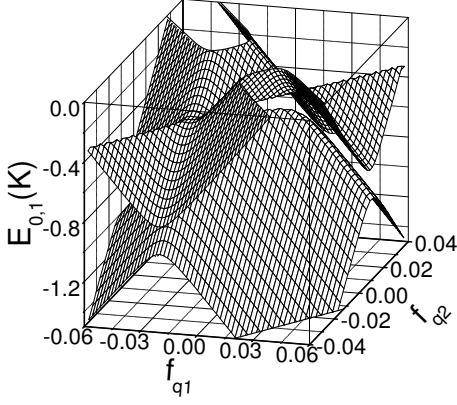


Fig. 2. The first two energy levels for an AFM-coupled two qubit system. Calculated for $I_{p,1} = 100$ nA, $I_{p,2} = 150$ nA, $\Delta_1 = \Delta_2 = 100$ mK and $J = 300$ mK.

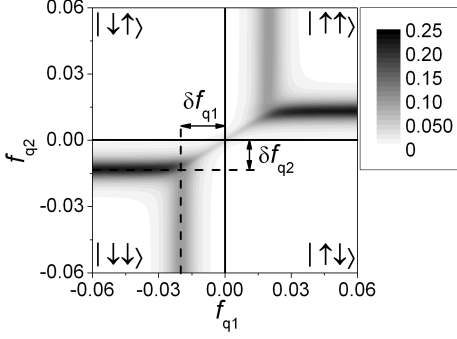


Fig. 3. $-\tan \Theta$ for an AFM-coupled two qubit system. The tank response is calculated for the same qubit parameters as used in Fig. 2. The read-out parameters are $L_T = 80$ nH, $M_{1,T} = M_{2,T} = 50$ pH and $Q_T = 500$ with an effective temperature $T = 70$ mK.

IV. EXPERIMENTAL IMPLEMENTATION

For our experiments we fabricate the qubit-system of interest inside a prefabricated superconducting planar coil made out of niobium on a Si chip. This coil forms the tank-circuit together with an external capacitor [15]. On the coil chip there are also Nb lines which allow the application of an asymmetric flux bias to the qubits. By applying a dc bias current I_{bT} through the tank and currents I_{b1} and I_{b2} (in the 3 qubit example shown in Fig. 1, 7a) through the lines we can separately change the magnetic flux in the qubits. For more qubits one should add additional lines.

As shown above, measuring the shift of the resonance frequency allows one to read-out the total susceptibility of the qubit system. Therefore, the tank-circuit is driven with a current $I_{\text{drive}}(t) = I_{ac} \cos(\omega t)$ at a frequency ω close to the resonance frequency ω_T of the tank circuit. The variation of the resonance frequency, due to the change in the susceptibility of the qubit system according to (6), can be measured by detecting the phase shift θ between the ac -current I_{drive} applied through the coil and ac -voltage over the tank circuit. This is realized by using the setup shown in Fig. 1. The voltage across the tank circuit is amplified by a cold HEMT-based amplifier followed by a room temperature amplifier. The phase shift Θ is measured using a lock-in amplifier with part of the signal which is used to bias the qubit used as a reference.

In the simplest case - one qubit at low temperature $k_B T \ll (E_\mu - E_\nu)/\hbar$, Φ_{tot} is proportional (through the mutual inductance) to the persistent current I_q flowing in the qubit system. Since a qubit is in the ground state E_0 the current I_q is proportional to $\frac{dE_0}{d\Phi_x}$. By taking into account Eq. 4 it can be easily shown that a shift of the tank resonant frequency due the tank-qubit interaction (and, therefore, $\tan \Theta$ or χ_{ij}) is proportional to the ground state curvature $\frac{d^2 E_0}{d\Phi_x^2}$. Because the ground state curvature is maximal near the anticrossing, the output signal as a function of the applied magnetic flux undergoes a narrow dip [16] at $\Phi_0/2$. From the shape of the dip the one-qubit Hamiltonian can be reconstructed by making use of the following equations [8]:

$$I_p = \frac{\tan \theta_{\text{max}} \Phi_0 F_{HW}}{k^2 Q L_q 2\sqrt{2^{2/3} - 1}}, \quad (8)$$

$$\Delta = I_p \frac{\Phi_0 F_{HW}}{2\sqrt{2^{2/3} - 1}}. \quad (9)$$

At higher temperatures one can fit the dip directly to the theory as given by Eqs. (6) and (7).

By properly biasing a multi qubit system one can use this single qubit reconstruction procedure for a multi qubit system. The bias to such an N qubit system is applied as follows: for $N - 1$ qubits $\epsilon_i \gg \Delta_i$ and $\epsilon_i \gg J_{i,j}$ for any j . Then the Δ_i in Eq. (1) for $N - 1$ qubits and also the interaction between all qubits can be neglected. Doing so reduces Eq. (1) to the Hamiltonian of a single qubit. The $N - 1$ qubits far from their degeneracy points can be considered as conventional classical magnetic moments and their influence on the N th qubit provides an additional bias $\epsilon_{N,\text{eff}}$ only. The resulting Hamiltonian is $H_q = -(\epsilon_{N,\text{eff}} + \epsilon_N) \sigma_z^{(N)} + \Delta_N \sigma_x^{(N)} + \text{Const.}$ Therefore, from measurements described above, and by making use of Eqs. (8), (9), the persistent current $I_{p,N}$ as well as Δ_N can be determined. By repeating this procedure for the other qubits we can find their parameters.

In order to complete the determination of the parameters of H_q the coupling energies J_{ij} must be obtained. They can be obtained from the shift of the qubit dips relative to the common degeneracy point. This can be seen in the numerically calculated energy levels and qubit response in Figs. 2 and 3. For low T and small Δ_i , the locations of the dips in $\tan \Theta(f_1, f_2, \dots)$, due to anti-crossings, simply follow the separation lines between the different classical states in the classical stability diagram. Due to this the state of the two-qubit system can be easily reconstructed. Moreover, the coupling energy follows directly from this stability diagram. For instance, the transition $|\uparrow\uparrow\rangle \longleftrightarrow |\downarrow\downarrow\rangle$ occurs at $\epsilon_1 = J$. Therefore, one can easily show that the coupling energy follows from $J = \delta f_{q1} \Phi_0 I_{p,1} = \delta f_{q2} \Phi_0 I_{p,2}$.

In Fig. 4 we show some quite recent results from a 2 qubit system measured with an improved setup. The qubits in this sample are coupled by a common Josephson junction as in Ref. [12]. This allows one to design the coupling strength over a wider range and than with inductive coupling only. By using the procedure described above all parameters of the Hamiltonian, Eq. 1, were found from the experimental data. The mutual inductances M_{iT} between the coil and qubits were

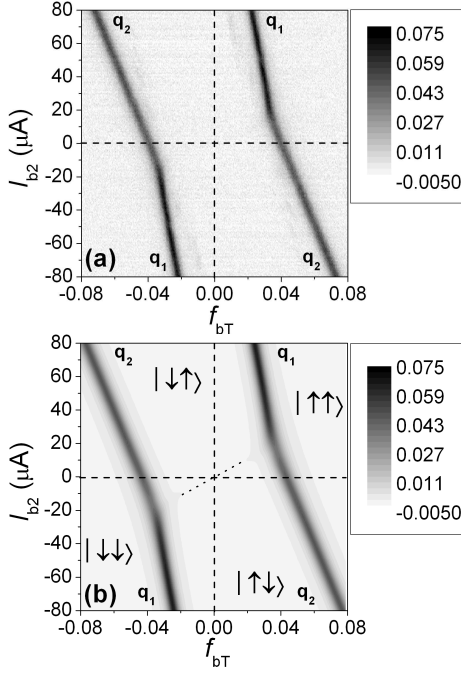


Fig. 4. (a) $-\tan \Theta(I_{b2}, I_{bT})$ for AFM-coupled qubits measured at the mixing chamber temperature of 10 mK. (b) Theoretical fit for an effective temperature $T_{\text{eff}} = 30$ mK and for the sample parameters $\Delta_1 = 45$, $\Delta_2 = 55$, $J = 550$ (all in mK) and $I_{p1} = 92$ nA, $I_{p2} = 84$ nA.

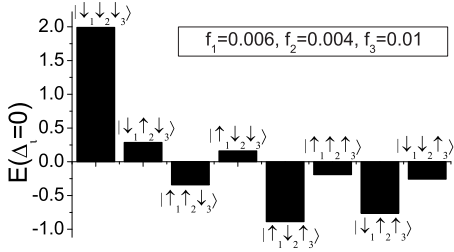


Fig. 5. Energy of the system for various vectors. $J_{12} = J_{23} = J_{13} = 0.3$ K. $\varepsilon_1 = 0.315$ K, $\varepsilon_2 = 0.252$ K, and $\varepsilon_3 = 0.525$ K. $|\uparrow_1\downarrow_2\uparrow_3\rangle$ is a global minimum, while $|\downarrow_1\uparrow_2\uparrow_3\rangle$ is a local one.

determined from the periodicity of the qubit signal from a scan over multiple Φ_0 . The mutual inductances between the bias lines and qubits followed from the slope of the qubit lines in Fig. 4a. These mutual inductances can be used to calculate the energy biases ε_i and, therefore, for the prediction of the response of the tank from the theory of Sec. III. This prediction is shown in Fig. 4b. The good agreement between experimental data and the theoretical prediction confirms the systems effective temperature of about 30 mK which also followed from the fit.

V. ADIABATIC QUANTUM COMPUTATION

In this section we review the AQC-algorithm for the solution of the MAXCUT problem. In particular we discuss a possible demonstration of AQC by making use of a system composed of three coupled flux-qubits using a resonant tank circuit for the readout.

Since the Hamiltonian of Eq. (1) is similar to an Ising Hamiltonian at $\Delta_i = 0$ it encodes the MAXCUT of a 3 vertex

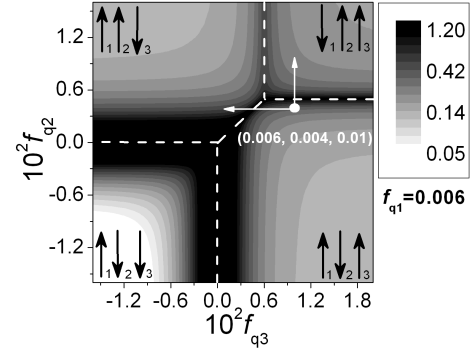


Fig. 6. $-\tan \Theta(f_{q2}, f_{q3})$ at $f_{q1} = 0.006$. The tank's response is calculated for $\Delta_1 = \Delta_2 = \Delta_3 = 96$ mK, $J_{12} = J_{13} = J_{23} = 300$ mK, $I_{p1} = I_{p3} = 350$ nA, $I_{p2} = 420$ nA, and $T = 10$ mK. The white dashed lines denote the cross-overs between the different classical states. At the white dot (0.006, 0.004, 0.01) the MAXCUT problem with the solution $|\uparrow_1\downarrow_2\uparrow_3\rangle$ is encoded, see Fig. 5. The solid arrows show the directions in which the read-out should be carried out in order to reconstruct this state.

graph if $\Delta_i/J_i \ll 1$ [8]. The simplest non-trivial case is a three-qubit system as shown in Fig. 1, for example with the following qubit parameters: $\Delta_1 = \Delta_2 = \Delta_3 = 96$ mK, $J_{12} = J_{13} = J_{23} = 300$ mK, $I_{p1} = I_{p3} = 350$ nA and $I_{p2} = 420$ nA. If this system is allowed to adiabatically evolve to the qubit energy biases $\varepsilon_1(0.006) = 0.315$ K, $\varepsilon_2(0.004) = 0.252$ K, and $\varepsilon_3 = 0.525(0.01)$ K, it will encode a MAXCUT problem with a solution given by the state $|\uparrow_1\downarrow_2\uparrow_3\rangle$. This can be seen in Fig. 5 where the energies of all flux-states for the Hamiltonian of Eq.(1) with all $\Delta_i = 0$, J_{ij} and ε_i as given above have been depicted. This system also exhibits a local minimum $|\downarrow_1\uparrow_2\uparrow_3\rangle$, two spin-flips away from the global minimum, this makes it an interesting test system for AQC. If a violation of the adiabatic evolution criterium occurs, the system can be found in this local minimum instead of the global one. This can be due to either thermal excitations during the readout or Landau-Zener transitions caused by a too high readout speed. Therefore one should optimize this readout speed depending on the energy gap in order to obtain optimal results.

The tank circuit response $-\tan \Theta(f_{q2}, f_{q3})$ predicted by Eqs. (6) and (7) for a fixed value $f_{q1} = 0.006$ is shown in Fig. 6. The white dashed lines denote the cross-overs between the different classical ($\Delta_i = 0$) states, which are marked in the figure by the state vectors $|\downarrow_1\uparrow_2\uparrow_3\rangle$, $|\uparrow_1\uparrow_2\downarrow_3\rangle$, $|\uparrow_1\downarrow_2\downarrow_3\rangle$ and $|\uparrow_1\downarrow_2\uparrow_3\rangle$. The main feature of the tank's response is that it restores the classical cross-overs. This fact can be used for reading out the state of the qubits at any flux point. In the case of Fig. 6 we want to know the qubits' configuration at (0.006, 0.004, 0.01), because this point encodes the solution of the MAXCUT problem that we are interested in. Therefore, if we perform the measurement of the qubits' susceptibility in the directions marked by solid arrows in Fig. 6, a *peak* structure will appear either to the left, or the right side of (0.006, 0.004, 0.01) in each flux direction. This allows the establishment of the following criterium: if the peak appears to the right(left) side of the starting point when we scan the flux f_{qi} through the qubit i , the starting point corresponds to the classical state \downarrow_i (\uparrow_i). Therefore, one can easily check that (0.006, 0.004, 0.01) corresponds to the $|\uparrow_1\downarrow_2\uparrow_3\rangle$ state if

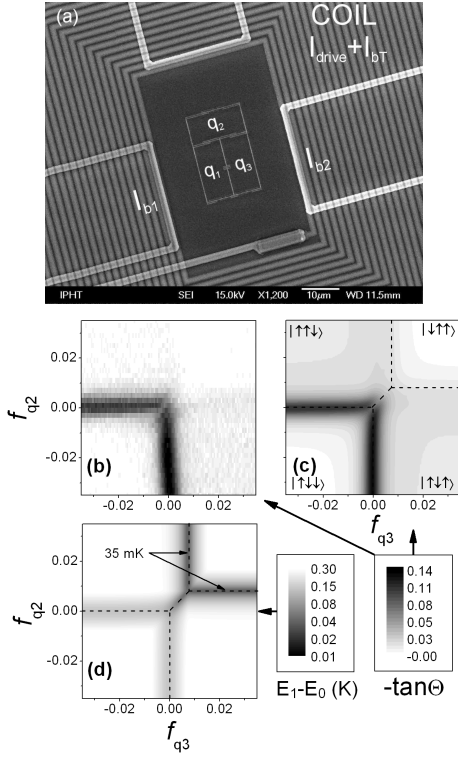


Fig. 7. (a) micrograph of the sample (b) $-\tan \Theta(f_{q2}, f_{q3})$ at $f_{q1} = 0.008$, measured at $T_{\text{mix}} = 10$ mK. (c) predicted response for $\Delta_1 = \Delta_2 = \Delta_3 = 70$ mK, $J_{12} = J_{13} = J_{23} = 610$ mK, $I_{p1} = I_{p2} = 115$ nA, $I_{p3} = 125$ nA, and $T_{\text{eff}} = 70$ mK. (d) Difference between the ground and first excited states. For (c) and (d) the black dashed lines denote the cross-overs between the different classical states.

all $\Delta_i = 0$ (for finding f_1 one would need another figure *e.g.* the (f_{q1}, f_{q3}) plane at a fixed value of $f_{q2} = 0.004$).

As a first step towards the demonstration of AQC we measured the full three-dimensional susceptibility of three anti-ferromagnetically coupled qubits [17]. For this purpose we fabricated a sample with the layout of Fig. 1 and measured it in our setup at a base temperature of 10 mK. Figure 7a shows a micrograph of the sample: three Al persistent current qubits are fabricated inside a Nb pancake coil. Two junctions in each qubit are nominally 600×120 nm², while a third one is $\sim 35\%$ smaller. Each qubit is coupled to the other two both magnetically and via shared 120×2000 nm² junctions. The flux through the qubits is controlled by direct currents through the coil I_{bT} , and two additional lines I_{b1} and I_{b2} (the third line was not used during the experiment). The Nb coil has an inductance $L_T = 134$ nH, and together with an external capacitance $C_T = 470$ pF forms a parallel tank circuit with $\omega_T/2\pi = 20.038$ MHz and quality $Q_T = 700$. The qubit-coil mutual inductances were extracted from the Φ_0 periodicity of the *ac*-susceptibility of the individual qubits as $M_{q1T} \approx 45.8$ pH and $M_{q2T} \approx 46.6$ pH, $M_{q3T} \approx 45.8$ pH. The mutual inductances between all qubits and biasing wires were found from two scans (I_{bT}, I_{b1}) , (I_{bT}, I_{b2}) , see Ref. [17].

Fig. 7b shows $-\tan \Theta(f_{q2}, f_{q3})$ at $f_{q1} = 0.008$, while Fig. 7c is the theoretical prediction for $\Delta_1 = \Delta_2 = \Delta_3 = 70$ mK, $J_{12} = J_{13} = J_{23} = 610$ mK, $I_{p1} = I_{p2} = 115$ nA, $I_{p3} = 125$ nA, and $T = 70$ mK. The experimental and

theoretical data are found to be in good agreement in the full three-dimensional flux space (other data for $f_{q1} = 0.005, 0, -0.005, -0.008$ can be found in [17]). However, for this sample not all classical cross-overs could be reconstructed. The narrow lines in the upper right quadrant of Fig. 7bc are absent. There are two main reasons for this: firstly the difference between the ground and first excited state (35 mK) along these measured lines is small (see Fig. 7d) in comparison with the effective temperature $T = 70$ mK for this measurements. Secondly all qubits' persistent currents (or magnetic moments) are similar, therefore there is no significant *magnetization* change along the transitions $|\uparrow_1\uparrow_2\downarrow_3\rangle \longleftrightarrow |\downarrow_1\uparrow_2\uparrow_3\rangle$ and $|\downarrow_1\uparrow_2\uparrow_3\rangle \longleftrightarrow |\uparrow_1\downarrow_2\uparrow_3\rangle$, thus there is no susceptibility change and no phase shift. In order to observe these lines, one could make a sample with different persistent currents, increase the gap between the ground and first excited states, or decrease the system's effective temperature. For the latter approach we already made some progress because for our improved experimental setup, see Fig. 4, we have reached an effective temperature ~ 30 mK.

The next steps for AQC will be a improving the read-out speed, the demonstration of the real adiabatic evolution/computation and demonstration of its efficiency in comparison with the classical simulated annealing.

VI. DISCUSSION

This review is concluded by answering some general questions that we have been often asked. The first question is whether it is possible to realize AQC with coupled classical magnetic moments? Or in other words: do we need quantum mechanics for an AQC implementation? In the quantum system there is an energy gap between the ground and the first excited states, thus the qubit system can evolve always staying in the ground state. A system without level- anticrossings exhibits many metastable states, so that evolution in the ground state is not possible.

As the qubits stability diagrams, shown in Figs. 3, 6 are the same as would be expected for coupled classical magnetic moments, where is the proof that the system described above behaves quantum mechanically? In the classical limit the persistent current “qubits” have a magnetic hysteresis for any finite qubit's inductance. This hysteresis was observed by making use of our method [18]. In this work instead of hysteresis we observed a narrow dip, which reflects the level anticrossing due to quantum tunneling. Therefore, there is a nonzero gap between the ground and the first excited state which allows AQC.

The stability of AQC against external noise, to our knowledge, is not known. On one hand, since we do not use any coherent oscillations, AQC should not be very sensitive to the environment. On the other hand, external noise can change the Hamiltonian itself and, therefore, its ground state. This issue requires further study.

In the present work we discussed our approach for demonstrating an adiabatic quantum algorithm by making use of a coupled flux-qubit system. By making use of a low-frequency resonator inductively coupled to the qubits we can completely reconstruct the parameters of a multi-qubit system. This multi-qubit ground state anticrossings read-out can be currently

performed at an effective temperature of 30 mK. The experimental data are found to be in complete agreement with quantum mechanical predictions. We have reconstructed the susceptibility of three coupled flux qubits in full parameter space. The next steps towards AQC will be improvement of the read-out speed and the demonstration of adiabatic quantum computation and its efficiency.

APPENDIX SUSCEPTIBILITY CALCULATION

Starting from the first order approximation of the total flux given in the main text (eq. 5) we can write out the commutator as a sum of the qubit response functions φ_{ij} :

$$\langle (i/\hbar)[\Phi(t), \Phi(t_1)]_- \rangle \theta(t - t_1) = \sum_{ij} \lambda_i \lambda_j \varphi_{ij}(t, t_1). \quad (10)$$

with

$$\varphi_{ij}(t, t_1) = \langle (i/\hbar)[\sigma_z^{(i)}(t), \sigma_z^{(j)}(t_1)]_- \rangle \theta(t - t_1), \quad (11)$$

where we introduced the Heaviside step function: $\theta(t - t_1) = 1$, if $t > t_1$, and $\theta(t - t_1) = 0$, when $t < t_1$.

For small values of the tank current and voltage the derivative of the total qubit flux is given by the expression

$$\frac{d}{dt} \langle \Phi_{tot}(t) \rangle = \sum_{ij} \frac{\lambda_i \lambda_j}{L_T} \int dt_1 \varphi_0(t, t_1) \langle V_T \rangle(t_1). \quad (12)$$

Putting this into Eq. (4) results in a shift of the resonant frequency of the tank which is proportional to the susceptibility and is just the Fourier transform of the response function:

$$\chi_{ij}(\omega) = \int d\tau e^{i\omega\tau} \varphi_{ij}(\tau). \quad (13)$$

This shift in the resonance frequency causes the phase shift when the tank is driven with its unloaded resonance frequency ω_T according to Eq. (6).

In order to calculate the linear response functions $\varphi_{ij}(t, t_1)$ (Eq. (11)) we have to find the product of two projections of Pauli matrices taken at times t and t_1

$$\langle \sigma_z^{(i)}(t) \sigma_z^{(j)}(t_1) \rangle = \sum_{\mu} \rho_{\mu} \langle \mu | \sigma_z^{(i)}(t) \sigma_z^{(j)}(t_1) | \mu \rangle, \quad (14)$$

averaged over the quantum-mechanical states $\langle \mu | \dots | \mu \rangle$ and the equilibrium distribution $\rho_{\mu} = e^{-E_{\mu}/k_B T} / (\sum_{\alpha} e^{-E_{\alpha}/k_B T})$.

As a result we obtain the expression

$$\begin{aligned} \varphi_{ij}(t, t_1) &= \varphi_{ij}(t - t_1) = (i/\hbar) \theta(t - t_1) \\ &\sum_{\mu} \rho_{\mu} \sum_{\beta} \{ \langle \mu | \sigma_z^{(i)} | \beta \rangle \langle \beta | \sigma_z^{(j)} | \mu \rangle e^{i\omega_{\mu\beta}(t-t_1)} - \\ &\langle \mu | \sigma_z^{(j)} | \beta \rangle \langle \beta | \sigma_z^{(i)} | \mu \rangle e^{i\omega_{\beta\mu}(t-t_1)} \}, \end{aligned} \quad (15)$$

for the linear response functions $\varphi_{ij}(t, t_1)$ (15). which give after Fourier transformation:

$$\begin{aligned} \chi_{ij}(\omega) &= - \sum_{\mu\nu} \frac{\rho_{\mu} - \rho_{\nu}}{\hbar\omega + E_{\mu} - E_{\nu} + i0} \\ &\langle \mu | \sigma_z^{(i)} | \nu \rangle \langle \nu | \sigma_z^{(j)} | \mu \rangle. \end{aligned} \quad (16)$$

By taking into account that the resonant frequency of the tank is much smaller than the level spacing and, therefore, can be neglected Eq. (7) of the main text is generated.

ACKNOWLEDGMENT

We thank D. V. Averin, A. Blais, A. Shnirman, E. Goldobin, Ya. S. Greenberg, R. Gross, H. E. Hoenig, Yu. A. Pashkin, M. J. Storz, F. K. Wilhelm and A. Zeilinger for fruitful discussions.

REFERENCES

- [1] E. Farhi, J. Goldstone, S. Gutmann, and M. Sipser, "Quantum computation by adiabatic evolution," quant-ph/0001106.
- [2] P. Bertet, I. Chiorescu, G. Burkard, K. Semba, C. J. P. M. Harmans, D. P. DiVincenzo, and J. E. Mooij, "Dephasing of a superconducting qubit induced by photon noise," *Phys. Rev. Lett.*, vol. 95, no. 25, pp. 257002, 2005.
- [3] F. Yoshihara, K. Harrabi, A. O. Niskanen, Y. Nakamura, and J. S. Tsai, "Decoherence of flux qubits due to 1/f flux noise," *Phys. Rev. Lett.*, vol. 97, no. 16, pp. 167001, 2006.
- [4] W. M. Kaminsky, S. Lloyd, and T. P. Orlando, "Scalable superconducting architecture for adiabatic quantum computation," quant-ph/0403090.
- [5] J. E. Mooij, T. P. Orlando, L. Levitov, L. Tian, C. H. van der Wal, and S. Lloyd, "Josephson persistent-current qubit," *Science*, vol. 285, pp. 1036–1039, 1999.
- [6] M. Steffen, W. van Dam, T. Hogg, G. Breyta, and I. Chuang, "Experimental implementation of an adiabatic quantum optimization algorithm," *Phys. Rev. Lett.*, vol. 90, no. 6, pp. 067903, 2003.
- [7] M. R. Garey, D. S. Johnson, and L. Stockmeyer, "Some simplified NP-complete graph problems," *Theor. Comput. Sci.*, vol. 1, pp. 237–267, 1976.
- [8] M. Grajcar, A. Izmailkov, and E. Il'ichev, "Possible implementation of adiabatic quantum algorithm with superconducting flux qubits," *Phys. Rev. B*, vol. 71, pp. 144501, 2005.
- [9] A. Izmailkov, M. Grajcar, E. Il'ichev, T. Wagner, H.-G. Meyer, A. Y. Smirnov, M. H. S. Amin, A. M. van den Brink, and A. M. Zagorskin, "Evidence for entangled states of two coupled flux qubits," *Phys. Rev. Lett.*, vol. 93, pp. 037003, 2004.
- [10] J. B. Majer, F. G. Paauw, A. C. J. ter Haar, C. J. P. M. Harmans, and J. E. Mooij, "Spectroscopy on two coupled superconducting flux qubits," *Phys. Rev. Lett.*, vol. 94, no. 9, pp. 090501, 2005.
- [11] L. S. Levitov, T. P. Orlando, J. B. Majer, and J. E. Mooij, "Quantum spin chains and Majorana states in arrays of coupled qubits," cond-mat/0108266.
- [12] M. Grajcar, A. Izmailkov, S. H. W. van der Ploeg, S. Linzen, E. Il'ichev, T. Wagner, U. Hübner, H.-G. Meyer, A. Maassen van den Brink, S. Uchaikin, and A. M. Zagorskin, "Experimental realization of direct Josephson coupling between superconducting flux qubits," *Phys. Rev. B*, vol. 72, no. 2, pp. 020503, 2005.
- [13] S. H. W. van der Ploeg, A. Izmailkov, A. Maassen van den Brink, U. Hübner, M. Grajcar, E. Il'ichev, H.-G. Meyer, and A. M. Zagorskin, "Controllable coupling of superconducting flux qubits," *Phys. Rev. Lett.*, vol. 98, no. 5, pp. 057004, 2007.
- [14] E. Il'ichev, A. Y. Smirnov, M. Grajcar, A. Izmailkov, D. Born, N. Oukhanski, T. Wagner, W. Krech, H.-G. Meyer, and A. Zagorskin, "Radio-frequency method for investigation of quantum properties of superconducting structures," *Fiz. Nizk. Temp.*, vol. 30, no. 30, pp. 823–833, 2004.
- [15] T. May, E. Il'ichev, H.-G. Meyer, and M. Grajcar, "Microfabricated oscillator for radio-frequency microscopy with integrated magnetic field concentrator," *Rev. Sci. Instr.*, vol. 74, no. 3, pp. 1282–1284, 2003.
- [16] Y. S. Greenberg, A. Izmailkov, M. Grajcar, E. Il'ichev, W. Krech, H.-G. Meyer, M. H. S. Amin, and A. Maassen van den Brink, "Low-frequency characterization of quantum tunneling in flux qubits," *Phys. Rev. B*, vol. 66, no. 21, pp. 214525, 2002.
- [17] A. Izmailkov, M. Grajcar, S. H. W. van der Ploeg, U. Hübner, E. Il'ichev, H.-G. Meyer, and A. M. Zagorskin, "Measurement of the ground-state flux diagram of three coupled qubits as a first step towards the demonstration of adiabatic quantum computation," *Europhys. Lett.*, vol. 76, no. 3, pp. 533–539, 2006.
- [18] E. Il'ichev, Th. Wagner, L. Fritzsche, J. Kunert, V. Schultze, T. May, H. E. Hoenig, H. G. Meyer, M. Grajcar, D. Born, W. Krech, M. V. Fistul, A. M. Zagorskin, "Characterization of superconducting structures designed for qubit realizations," *Appl. Phys. Lett.*, vol. 80, pp. 4184–4186, 2002.